Biointerface Research in Applied Chemistry
Open-Access Journal (ISSN: 2069-5837)

Article
Volume 13, Issue 6, 2023, 572
https://doi.org/10.33263/BRIAC136.572

Investigation of Nucleation and Growth Mechanism of Bi-Doped ZnO Electrodeposited on ITO Substrate

Youssef Lghazi [1],[*], Jihane Bahar [1], Chaimaa El haimer [1], Boubaker Youbi [1], Aziz Aynaou [1], Ahmed Sahlaoui [1], Abdessamad Ouedrhiri [1], Mohammed Ait Himi [1], Mohamed Ouknin [2], Itto Bimaghra [1], Lhou Majidi [2,*]

[1] Laboratory Bio-Geosciences and Materials Engineering, Ecole Normale Supérieure, Hassan II University of Casablanca, Casablanca, Morocco
[2] Laboratory of Natural Substances Synthesis and Molecular Dynamics, Faculty of Sciences and Techniques, Moulay Ismail University, Errachidia, Morocco
* Correspondence: l.majidi@fste.umi.ac.ma or lmajidi@yahoo.fr (L.M.);

Scopus Author ID 15760507800
Received: 19.11.2022; Accepted: 9.01.2023; Published: 26.03.2023

Abstract: The Bi-doped zinc oxide (Bi-ZnO) nanostructured was elaborated on the indium-doped tin oxide (ITO) substrate by electrodeposition. The bath temperature was performed at 70°C. The films were cathodically electrodeposited in a bath containing 0.01mol.L^{-1} $Zn(NO_3)_2$. $6H_2O$, while the source of doping is $Bi(NO_3)_3$. $5H_2O$ and 0.1 mol.L^{-1} KNO_3 was used as supporting electrolyte. Our interest is to study the influence of doping on the mechanism of electrodeposition and the structural and optical properties of these layers. The cyclic voltammetry and chronoamperometry investigation shows that the electrodeposition of ZnO and Bi ZnO doped at a negative potential around −1.1 V versus Ag/AgCl is a quasi-reversible reaction controlled by the diffusion process. Current transient curves measured showed that the nucleation mechanism of ZnO and Bi-doped ZnO is instantaneous with three-dimensional growth of hemispherical nuclei. XRD patterns show that ZnO and Bi-doped ZnO on the ITO substrate crystallizes in a hexagonal würtzite-like structure. UV-Visible transmission spectrum affirms that good transparent films of Bi-doped ZnO cannot be obtained. SEM analysis revealed that the morphology of the obtained deposits depends on the type of electrodeposition mechanism.

Keywords: zinc oxide; bismuth; electrodeposition; cyclic voltammetry; chronoamperometry; nucleation and growth.

1. Introduction

Zinc oxide (ZnO) is a semiconductor; it exhibits a wide band gap of 3.3 eV and a high exciton binding energy of 60 meV [1] at ambient temperature, as well as excellent catalytic, optical, electrical, optoelectronic, gas sensing, piezoelectric, and photoelectrochemical properties [2,3]. Currently, ZnO is used in numerous applications, including solar cells [4], light-emitting diodes [5], waveguides [6], and lasers [7]. On the other hand, zinc oxide (ZnO) is a piezoelectric and moisture-sensitive material that has been explored as an active layer in nanogenerators [8] and humidity sensors [9]. Several techniques are used to obtain ZnO and Bi-doped ZnO films, such as sol-gel methods [10], spray pyrolysis [11], chemical vapor deposition (CVD) [12], and electrodeposition [13]. Today, the electrodeposition technique is an important method for preparing thin semiconductor films. The preparation of oxide films by electrodeposition from an aqueous solution has several advantages over other techniques; this

method is conducted at low temperatures. In this paper, ZnO and Bi-doped ZnO thin films were electrodeposited from zinc nitrate hexahydrate solution while the doping source is bismuth nitrate pentahydrate on the ITO substrate. ZnO is a group II-VI semiconductor, and doping certain minor elements in its matrix can significantly affect its properties. However, the electrochemical technique used was a good choice, as indicated previously. In the literature, people have used an electrochemical method to deposit ZnO films doped with elements such as Al, Co, In, Bi… to improve the properties of thin ZnO films [14]. This work aims to study the mechanism of electrodeposition and the effect of the doping rate by bismuth on the structural and optical properties of ZnO films.

2. Materials and Methods

2.1. Electrochemical measurements.

Electrochemical measurements were performed using a three-electrodes cell configuration connected to Versa STAT 3 potentiostat/galvanostat supported by a computer using the versa studio software. ITO (tin (Sn) doped indium oxide (In_2O_3)) substrate with a surface area of 1 cm^2 was used as a working electrode; the platinum electrode was used as a counter electrode and Ag/AgCl as a reference electrode (all potentials are given versus Ag/AgCl). The ZnO and Bi-doped ZnO nanostructures films were cathodically electrodeposited from baths containing different molar ratios of $Zn(NO_3)_3.6H_2O$ in 0.01M, while the source of doping is $Bi(NO_3)_2$. $5H_2O$, the doping rate was varied from 0 to 10 % Bi, and 0.1 M potassium nitrate (KNO_3) as the supporting electrolyte. The solutions used were freshly prepared with distilled water. The bath temperature was kept at 70 °C for all measurements.

2.2. Films characterization and analysis.

The structure of the thin films of ZnO and Bi-doped ZnO has been determined by X-ray diffraction (XRD) analysis using a Broker D8 Advance diffractometer equipped with a graphite monochromator, a Lynx-Eye detector, and parallel beam optics Cu Kα radiation (λ= 1.5411 Å). The UV–visible transmittance spectra have been recorded with a Shimadzu UV-1800 UV/visible Scanning Spectrophotometer. The scanning electron microscopy (SEM) observations were performed using a Philips XL 30FEG.

3. Results and Discussion

3.1. Cyclic voltammetry.

The investigation of the electrodeposition kinetics of ZnO and Bi-doped ZnO on ITO substrate was performed mainly using the cyclic voltammetry (CV) method for a different doping rate. The cyclic voltammetry in Figures 1(a) and (b) show the electrodeposition chemical behavior during ZnO and Bi-doped ZnO electrodeposition on ITO substrate. The CV curves recorded between 0 and -1.4V versus Ag/AgCl are related to the deposition and dissolution of metals.

The thin films were electrodeposited from two electrolyte baths; the first contained $Zn(NO_3)_2$. $6H_2O$ (0.01M) with potassium nitrate KNO_3 (0.1 M) for electrodeposited of ZnO on ITO substrate, the second one contains $Zn(NO_3)_2$. $6H_2O$ (0.01 M), while the source of doping

is $Bi(NO_3)_3$. $5H_2O$, the doping rate was varied from 0 to 10 % Bi and potassium nitrate KNO_3 (0.1M) for electrodeposition of Bi-doped ZnO on ITO substrate.

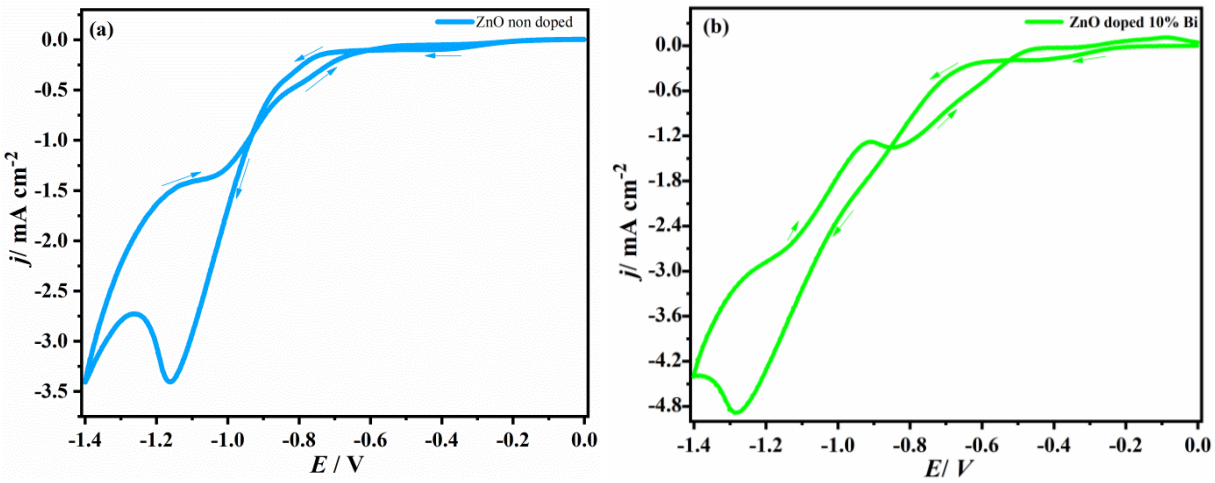

Figure 1. Cyclic voltammograms:**(a)** ZnO alone and **(b)** ZnO doped 5 % Bi electrodeposited on ITO substrate at 50 mV. s^{-1}.

Cyclic voltammetry (CV) in Figure 1(a) was performed to study the electrochemical reduction of ZnO. During the forward scan, the reduction of Zn_2^+ leads to a metallic deposition of Zn at the potential (E= -0.3 V vs. Ag/AgCl) following equation (1). Furthermore, the electrochemical formation mechanism of ZnO is known to initiate by the reduction of nitrate ions (NO^{3-}) at potential (E= -0.8 V vs. Ag/AgCl), which produces hydroxide ions (OH), followed by the precipitation of $Zn(OH)_2$. The conversion of $Zn(OH)_2$ to ZnO happens in an ultimate step due to the effect of temperature [15]. The ZnO deposition sequence can be summarized by the following equations (2, 3, and 4):

$$Zn_2^+ + 2e^- \leftrightharpoons Zn \quad (1)$$

$$NO_3^- + H_2O + 2e^- \leftrightharpoons NO^{2-} + 2HO^- \quad (2)$$

$$Zn_2^+ + 2\ OH^- \leftrightharpoons Zn(OH)_2 \quad (3)$$

$$Zn(OH)_2 \leftrightharpoons ZnO + H_2O \quad (4)$$

Corresponding to the overall reaction:

$$NO^{3-} + Zn^{2+} + 2e^- \rightarrow NO^{2-} + ZnO \quad (5)$$

Based on Figure 1(a), it is evident that the cathodic reduction system observed at the potential (E= -1.3 V vs. Ag/AgCl) corresponds to the reduction of water according to equation (6).

$$H_3O^+ + 1e^- \leftrightharpoons 1/2\ H_2 + H_2O \quad (6)$$

Figure 1(b) shows the CV electrodeposition of Bi-doped ZnO. We observed the same peaks as in Figure 1(a). Moreover, when scanning forward, the reduction of Bi^{3+} leads to a metallic Bi deposit at potential (E= -0.7Vversus Ag/AgCl) according to equation (7), and when scanning back, the oxidation of Bi to Bi^{3+} at potential (E= -0.2Vversus Ag/AgCl) according to equation (8):

$$Bi^{3+} + 3e^- \leftrightharpoons Bi \quad (7)$$

$$Bi \leftrightharpoons Bi^{3+} + 3e^- \quad (8)$$

Moreover, the electrochemical formation mechanism of Bi_2O_3 is known to be initiated by the reduction of nitrate ions (NO_3^-) that produce hydroxide ions (OH-), followed by the precipitation of $Bi(OH)_3$. The conversion of $Bi(OH)_3$ into Bi_2O_3. ZnO deposition sequence can be summarized by the following equations (2, 9, and 10):

$$Bi^{3+} + 2\ OH^- \leftrightharpoons Bi(OH)_3 \quad (9)$$

$$2\ Bi(OH)_2 \leftrightharpoons Bi_2O_3 + 3H_2O \quad (10)$$

Each curve displays a crossover. The presence of this crossover gives rise to what has been called the "nucleation loop" which indicates the formation of ZnO nucleation on ITO substrate in Figure 1(a) and the formation of Bi-doped ZnO nucleation on ITO substrate in Figure 1(b) [16].

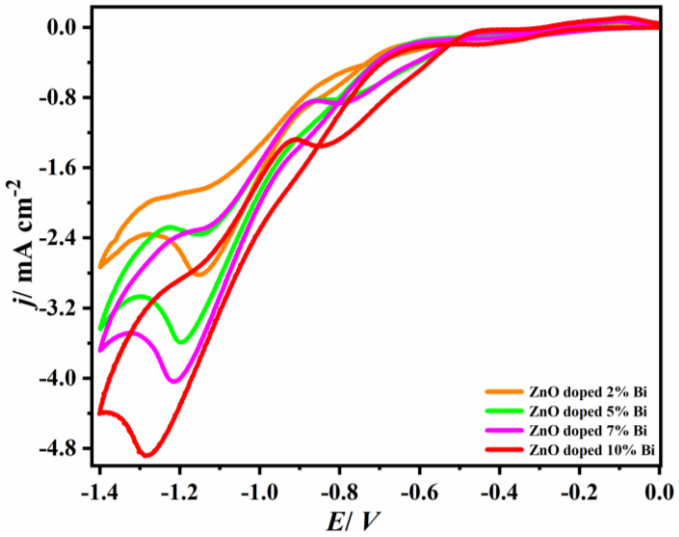

Figure 2. Cyclic voltammograms of co-deposition ZnO-Bi at different doping rates (2% Bi, 5% Bi, 7% Bi and 10%Bi) electrodeposited on ITO substrate.

Figure 2 illustrates a series of cyclic voltammograms for Bi-doped ZnO at different doping rates (2% Bi, 6% Bi, 7% Bi and 10% Bi) electrodeposited on ITO substrate. When scanning towards the cathodic potentials, we observe an increase in the peak intensity attributed to the electrodeposition of ZnO according to the doping rate and its displacement towards the most cathodic potential. During the return scan towards the anodic potentials, an increase in the peak intensity attributed to the oxidation of Bi according to the doping rate and its displacement towards the most anodic potential.

3.2. Chronoamperometry.

Chronoamperometry is an electrochemical technique to study the early stages of electrodeposition [17]. The study by chronoamperometry is carried out at -1.1V versus Ag/AgCl for electrodeposition of ZnO alone and doped ZnO with different doping rates of Bi. The series of current density time transients are shown in Figure 3 for different doping rates of Bi (0% Bi, 2% Bi, 6% Bi, 7% Bi, and 10% Bi).

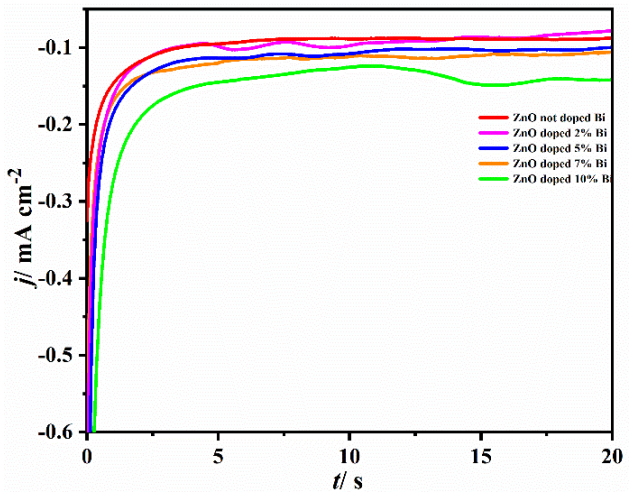

Figure 3. Current transients of ZnO alone and Bi-doped ZnO electrodeposited on ITO substrate.

Figure 3 shows a series of current transients for ZnO alone and Bi-doped ZnO at a different doping rate (2% Bi, 5% Bi, 7% Bi and 10% Bi) electrodeposited on ITO substrate at potential (*E*= -1.1V versus Ag/AgCl). The transients' current density-time obtained show the typical shape of a three-dimensional (3D) nucleation mechanism for ZnO alone and co-deposition Bi-ZnO. The transients present an ascending part between 0 s and 3s, corresponding to the growth of germs, followed by a part in which the current density remains constant for the electrodeposition of ZnO alone. For t > 3s the current density in the transients of different doping rates of Bi is not constant, but we observe an increase and a decrease of the current density with time; this behavior could be explained by the fact that the co-deposition mechanism of Bi-ZnO is done layer by layer.

3.2.1. Exploitation of the ascending part.

Scharifker and Hills have developed theoretical models describing the 3D nucleation mechanism. For instantaneous nucleation, nuclei are formed at the beginning of the pulse, but for the progressive one, the nuclei are continuously formed during the crystal growth. The variation of the current density in the ascending part on the current transients can be described by the following equations (11 and 12) [18-27].

For instantaneous 3D nucleation: $$j(t) = nF\pi(2DC)^{3/2}(M/\rho)^{1/2}Nt^{1/2} \quad (11)$$

For progressive 3D nucleation: $$j(t) = \frac{2}{3}nF\pi(2DC)^{3/2}(M/\rho)^{1/2}ANt^{3/2} \quad (12)$$

With $j(t)$ represents the current density (Acm^{-2}), C represents the concentration of electroactive ions (mol.cm-3), D is the diffusion coefficient ($cm^2.s^{-1}$), F is the Faraday constant (96500 C. mol^{-1}), n is the number of electrons transferred in the electrodeposition process, M is the molar mass of the deposit ($g.mol^{-1}$), ρ is the density of the deposit ($g.cm^{-2}$), A is the nucleation rate constant (s^{-1}), and N is the number density of nuclei (cm^{-2}).

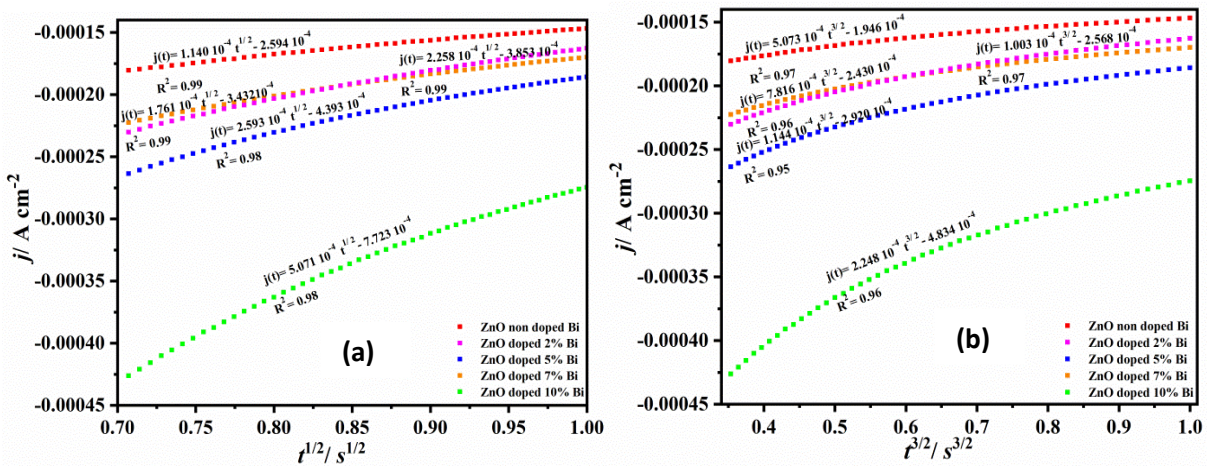

Figure 4. (a) $j(t)$ vs. $t^{1/2}$ plots at different doping rates of Bi and **(b)** $j(t)$ vs. $t^{3/2}$ plots at different doping rates of Bi.

In accordance with equations (11) and (12), for all the transients presented in Figure 3, the experimental currents density of the ascending part of the transients were plotted versus $t^{1/2}$ and $t^{3/2}$ in Figures 4(a) and (b). As seen on all the different doping rates of Bi at potential -1.1V versus Ag/AgCl, the plots $j(t)$ vs. $t^{1/2}$ display a good linear relationship with higher correlation factors values than the ones of $j(t)$ vs. $t^{3/2}$ plots. This suggests that the mechanism of ZnO and Bi-doped ZnO electrodeposited under these conditions follows instantaneous 3D nucleation [20].

3.3. Crystal structure determination.

The X-ray diffraction patterns of the elaborated sample with the electrodeposition method at E = -1.2V versus Ag/AgCl, are presented in Figure 5 for ZnO alone and Bi-doped ZnO at different doping rates (2% Bi, 6% Bi, 10% Bi) electrodeposited on ITO substrate. As can be seen, the diffraction peaks at 2θ=34.43°, 47.26°, 63.52°, and 72.45° are characteristic of ZnO alone with a hexagonal structure which orientations have been preferred (002), (102), (103) and (004). For the diffractograms of Bi-doped ZnO, we observe the same peak of ZnO. Moreover, we observe new peaks that attributed to the Bi at 2θ = 31.69°, 34.43°, and 72.45° with preferred orientations (101), (210), and (43-2).

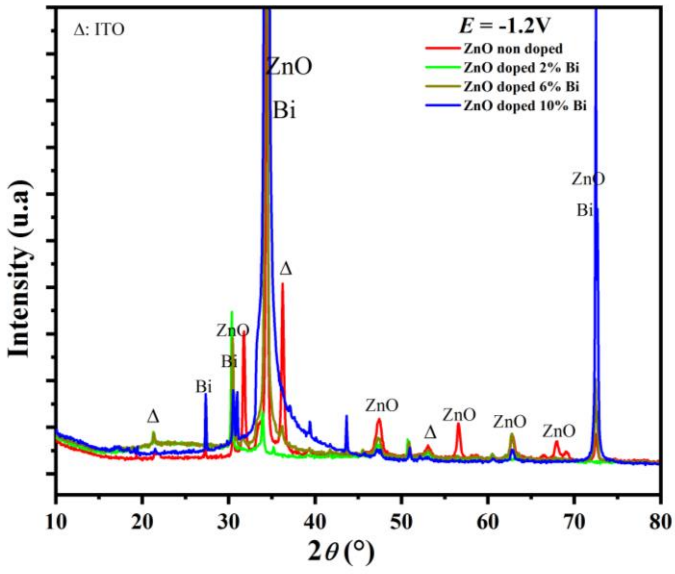

Figure 5. X-ray diffraction patterns of ZnO alone and Bi-doped ZnO at different doping rates.

The diffractograms of Bi-doped ZnO indicate a new secondary crystal phase of oxide of bismuth (Bi_2O_3) formed during electrodeposition processes at 2θ= 34.43°, whose preferred orientation was (200). The film obtained from ZnO alone is polycrystalline with a hexagonal wurtzite structure. The specter's XRD indicated that the bismuth doping does not change the wurtzite structure of ZnO. We can see that the intensity of the peak at 2θ=34.43° increases with the increase in the percentage of bismuth. The peak intensity (002) increases proportionally with the doping rates of Bi up to the achievement of the maximum, which is 10 % of Bi. The ionic radius of Zn_2^+ is about 0.74 Å, and Bi^{3+} is about 0.96 Å. Layer parameters for pure ZnO are a = 3.242 Å and c = 5.176 Å. In the case of Bi-doped ZnO, these parameters are a = 3.258 Å and c = 5.200 Å, which can be explained by the fact that the larger Bi ion is substituted in the ZnO lattice.

3.4. Optical proprieties.

UV-Visible Spectrophotometry is an optical characterization technique. It provides information on the optical effects of doping rates properties of the sample to be analyzed, such as the transmission and absorption of light and estimation of the optical gap. It can also inform us, in some cases, about the thickness of the sample.

In order to examine the properties of Bi-doped ZnO layers, we studied the evolution of the transmission spectra and the optical gap as a function of doping rate (2, 6, and 10% Bi).

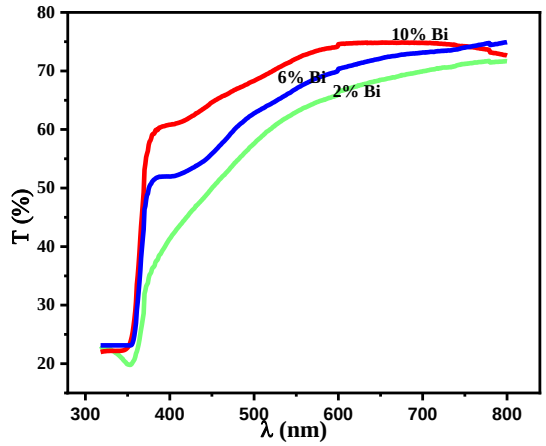

Figure 6. Transmission spectra of ZnO alone and Bi-doped ZnO prepared at different doping rates.

Figure 6 shows the transmittance spectra for Bi-doped ZnO electrodeposited on ITO substrate at 70 °C. As can be seen, all the films are transparent with a transmittance in the visible domain, which is important for the ZnO applications.

From to band theory, the relationship between the absorption coefficient α_{op} and the energy of the incident light hυ provides access to the gap energy of a semiconductor as given by the Tauc's:

$$(\alpha_{op}h\upsilon)^2 = B.(h\upsilon - Eg) \quad (13)$$

where B is a constant, Eg is the band gap, α_{op} is the absorption coefficient, hυ is the photon energy, and the plots of $(\alpha_{op}h\upsilon)^2$ with photon energy hυ are shown in Figure 7; it found to be linear over a wide range of photon energies indicating the indirect type of transition. The band gap of Bi-doped ZnO electrodeposition on ITO substrate has been calculated from the intercept of the plot on the energy axis. We see that the gap decreases with the percentage of Bi, contrary to what we found with cobalt doping [15]. This result is due to the fact that Bi is a group IIIB element, which is generally n donors.

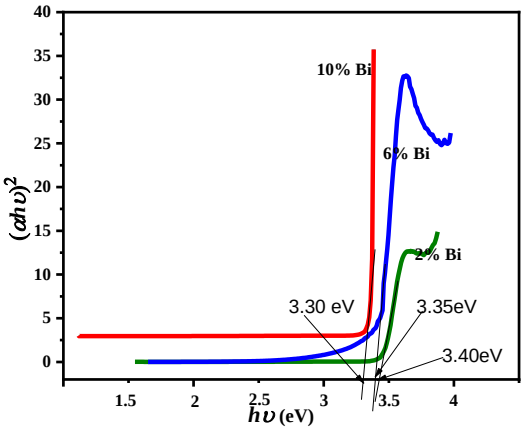

Figure 7. Plot of $(\alpha_{op}h\upsilon)^2$ versus $(h\upsilon)$.

3.4.1. Scanning Electron Microscopy.

Scanning electron microscopy (SEM) is a microscopy technique for obtaining relief images of the surface of samples with high resolution, ranging from 0.4 nm to 10 nm and greatly exceeding that of optical microscopy. Figures 8 and 9 represent a morphological study for samples, one for ZnO alone and the others for Bi-doped ZnO at different doping rates electrodeposited on ITO substrate at -1.2V versus SCE during 30 min.

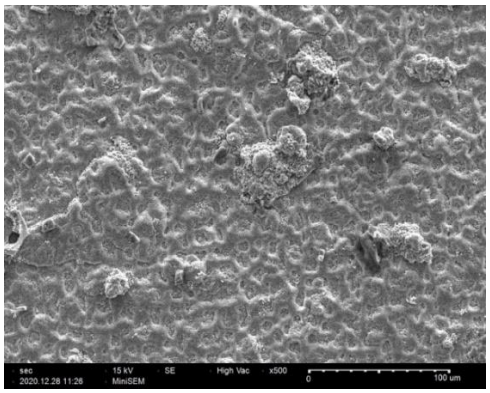

Figure 8. SEM image of ZnO alone electrodeposited for 30 min on ITO substrate at a potential of 1.2V/SCE.

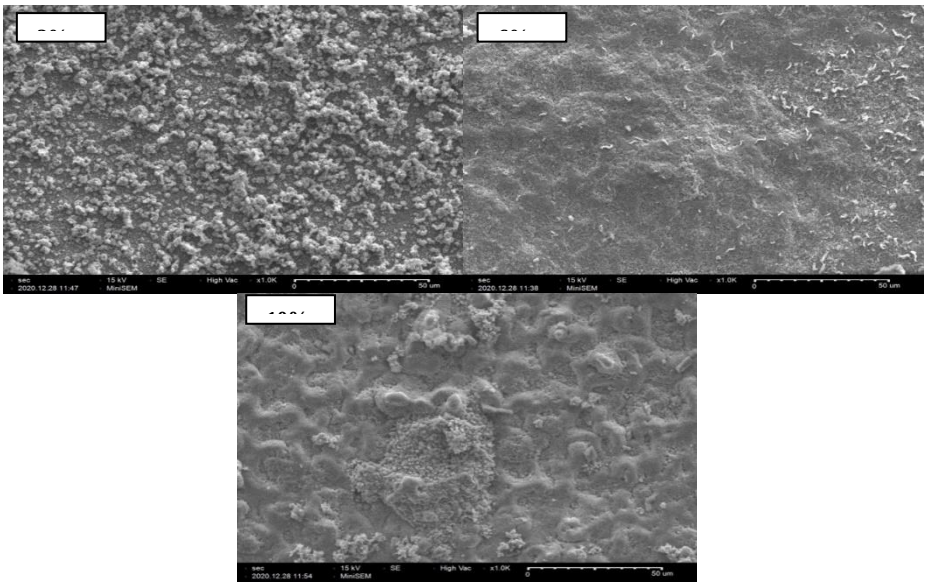

Figure 9. SEM image of Bi-doped ZnO (2% Bi, 6% Bi, and 10% Bi) electrodeposited for 30 min on ITO substrate at a potential of 1.2V/SCE.

Figures 8 and 9 demonstrate that the deposit of ZnO and Bi-doped ZnO at different doping rates is heterogeneous over the entire surface of the substrate, and the grains are all of different sizes and shapes. We can say that the morphology depends on the bismuth doping rates. We notice that the substrate surface is not completely covered by the deposit of ZnO and Bi-doped ZnO, which confers that the nucleation mechanism is progressive 3D.

4. Conclusions

In this paper, Bi-doped ZnO nanorod films were synthesized by electrodeposition method on ITO substrate. Effects of doping rates on the electrodeposition mechanism and structural, optical, and morphological properties are studied. The cyclic voltammetry investigation showed that the ZnO-doped Bi electrodeposition on the ITO substrate process is quasi-reversible and controlled by diffusion. The chronoamperometry method indicated that the electrodeposition nucleation and growth mechanism of ZnO and Bi-doped ZnO is achieved through a 3D progressive nucleation process. The X-ray diffraction characterization indicated that the ZnO and Bi-doped ZnO electrodeposition crystallized with a wurtzite structure. Band gap measurements using transmission spectra indicate that the ZnO films have a band gap of 3.9 eV, and when doping with Bi, the transmission spectra show a decrease in gap energy with increasing Bi rates.

Funding

This research received no external funding.

Acknowledgment

This work is carried out at the Bio-Geosciences and Materials Engineering research laboratory at the ENS Casablanca, Morocco. The authors would like to thank those who helped them carry out the XRD analysis at the faculty of sciences Ain Chock, Casablanca.

Conflicts of Interest

The authors declare no conflict of interest.

References

1. Mihailovic, M.; Henneghien, A.L.; Faure, S.; Disseix, P.; Leymarie, J.; Vasson, A.; Buell, D.A.; Semond, F.; Morhain, C.; Pérez, J.Z. Optical and excitonic properties of ZnO films. *Optical Materials* **2009**, *31*, 532-536, https://doi.org/10.1016/j.optmat.2007.10.023.
2. Yao, K.X.; Zeng, H.C. Asymmetric ZnO nanostructures with an interior cavity. *J. Phys. Chem. B* **2006**, *110*, 14736-14743, https://doi.org/10.1021/jp062751e.
3. Wang, Z.L.; Song, J. Piezoelectric nanogenerators based on zinc oxide nanowire arrays. *Scienc*, **2006**, *312*, 242-246, https://doi.org/10.1126/science.1124005.
4. Boukhoubza, I.; Matei, E.; Jorio, A.; Enculescu, M. ; Enculescu, I. Electrochemical Deposition of ZnO Nanowires on CVD-Graphene/Copper Substrates. *Nanomaterials* **2022**, *12*, 2858, https://doi.org/10.3390/nano12162858.
5. Aynaou, A.; Youbi, B.; Lghazi,Y.; Ait himi, M.; Bahar, J.; El haimer, C.; Ouedrhiri, A.; Bimaghra, I. «Nucleation, growth and electrochemical performances of polyaniline electrodeposited on ITO substrate», *J. Electrochem. Soc*. **2022**, *169*, 082509. https://doi.org/10.1149/1945-7111/ac862a.
6. Tsai, Y.S.; Tsai, S.C.; Kuo, C.C.; Chan, W.L.; Lin, W.H.; Wu, Y.S.; Lin, Y.S.; Li, M.H.; Kuo, M.Y.; Chen, H. Organic/inorganic hybrid nanostructures of polycrystalline perylene diimide decorated ZnO nanorods

highly enhanced dual sensing performance of UV light/CO gas sensors. *Results Phys.* **2021**, *24*, 104173, https://doi.org/10.1016/j.rinp.2021.104173.
7. Shafiee, P.; Nafchi, M.R.; Eskandarinezhad, S.; Mahmoudi, S.; Ahmadi, E. Sol-gel zinc oxide nanoparticles: advances in synthesis and applications. *Sci. Sinter.* **2021**, *1*, 242-254, https://doi.org/10.53063/synsint.2021.1477.
8. Serairi, L.; Leprince-Wang, Y. ZnO Nanowire-Based Piezoelectric Nanogenerator Device Performance Tests. *Crystals* **2022**, *12*, 1023, https://doi.org/10.3390/cryst12081023.
9. Bu, I.Y.; and Yang, C.C. High-performance ZnO nanoflake moisture sensor. *Superlattices Microstruct.* **2012**, *51*, 745-753, https://doi.org/10.1016/j.spmi.2012.03.009.
10. Mousavi, S.M.; Behbudi, G.; Gholami, A.; Hashemi, S.A.; Nejad, Z.M.; Bahrani, S.; Chiang, W.H.; Wei, L.C.; Omidifar, N. Shape-controlled synthesis of zinc nanostructures mediating macromolecules for biomedical applications. *Biomater. Res.* **2022**, *26*, 1-20, https://biomaterialsres.biomedcentral.com/articles/10.1186/s40824-022-00252-y.
11. El Jouad, M.; Garmim, T.; Louardi, A.; Hartiti, B.; Monkade, M.; Touhtouh, S.; Hajjaji, A. Elaboration and characterization of Ni and Al co-doped SnO_2 thin films prepared by spray pyrolysis technique for photovoltaic applications. *Mater. Sci. Eng. B* **2022**, *286*, 116044, https://doi.org/10.1016/j.mseb.2022.116044.
12. Ataev, B.M.; Bagamadova, A.M.; Mamedov, V.V.; Omaev, A.K. Thermally stable, highly conductive, and transparent ZnO layers prepared in situ by chemical vapor deposition. *Mater. Sci. Eng. B*, **1999**, *65*, 159-163, https://doi.org/10.1016/S0921-5107(99)00166-X.
13. Manzano, C.V.; Philippe, L.; Serrà, A. Recent progress in the electrochemical deposition of ZnO nanowires: synthesis approaches and applications. *Crit. Rev. Solid State Mater. Sci.* **2022**, *47*, 772-805, https://doi.org/10.1080/10408436.2021.1989663.
14. Okonkwo, B.O.; Jeong, C.; Jang, C. Advances on Cr and Ni Electrodeposition for Industrial Applications—A Review. *Coating* **2022**, *12*, 1555, https://doi.org/10.3390/coatings12101555.
15. Lghazi, Y.; Bahar, J.; Youbi, B.; Himi, M.A.; Elhaimer, C.; Elouadrhiri, A.; Bimaghra, I.; Ouknin, M.; Majidi,L. Nucleation/Growth and Optical Proprieties of Co-doped ZnO Electrodeposited on ITO Substrate. *Biointerface Res. Appl. Chem.* **2022**, *12*, 6776-6787, https://doi.org/10.33263/BRIAC125.67766787.
16. Li, D.; Zhao, C.; Doherty, A.; Yuan, S.; Gong, Y.; Wang, Q. Nucleation and growth mechanism of dendrite-free Ni–Cu catalysts by magneto-electrodeposition for the hydrogen evolution reaction. *New J. Chem.* **2022**, *46*, 5246-5255, https://doi.org/10.1039/D1NJ05967J.
17. Mashreghi, A.; Zare, H. Investigation of nucleation and growth mechanism during electrochemical deposition of nickel on fluorine doped tin oxide substrate. *Curr. Appl. Phys.* **2016**, *16*, 599-604, https://doi.org/10.1016/j.cap.2016.03.008.
18. Bahar, J.; Lghazi, Y.; Youbi, B.; Himi, M.A.; El Haimer, C.; Ouedrhiri, A.; Aynaou, A.; Bimaghra, I. Nucleation and growth mechanism of cuprous oxide electrodeposited on ITO substrate. *Mater. Today* **2022**, *66*, 187-195, https://doi.org/10.1016/j.matpr.2022.04.445.
19. Bahar, J.; Lghazi, Y.; Youbi, B.; Ait Himi, M.; Bimaghra, I. Comparative study of nucleation and growth mechanism of cobalt electrodeposited on ITO substrate in nitrate and chloride electrolytes. *J. Solid. State Electrochem.* **2021**, *25*, 1889-1900, https://doi.org/10.1007/s10008-021-04961-7.
20. Lghazi, Y.; Bimaghra, I.; Bachiri, A.; Elmerzouki, K.; Youbi, B.; Lasri, H. Investigation of the nucleation kinetics of Bi and Δ-Bi2O3 during electrodeposition on substrate ITO. *Int. J. Eng. Technol.* **2018**, *7*, 21-24.
21. Astley, D.J.; Harrison, J.A; Thirsk, H.R. Electrocrystallization of mercury, silver and palladium. *Trans. Faraday Soc.* **1968**, *64*, 192-201, https://doi.org/10.1039/TF9686400192.
22. Gunawardena, G.; Hills, G.; Scharifker, B. Induction times for the formation of single mercury nuclei on a platinum microelectrode. *J. electroanal. chem. interfacial electrochem.* **1981**, *130*, 99-112, https://doi.org/10.1016/S0022-0728(81)80379-8.
23. Youbi, B.; Lghazi, Y.; El Bachiri, A.; Himi, M.A.; Elibrizy, O.; Bimaghra, I. Investigation of nucleation and growth mechanism of bismuth electrodeposited on ITO substrate in nitric acid medium. *Mater. Today*, **2020**, *22*, 6-11, https://doi.org/10.1016/j.matpr.2019.08.055.
24. El haimer, C.; Lghazi, Y.; Bahar, J.; Youbi, B.; Ait himi, M.; Aynaou, A.; Bimaghra, I. electrochemical properties of Bi_2Se_3 layers semiconductor elaborated by electrodeposition, *J. Electroanal. Chem.* **2022**, 925, *15*, 116906 https://doi.org/10.1016/j.jelechem.2022.116906.
25. Monshi, A.; Foroughi, M.R.; Monshi, M.R. Modified Scherrer equation to estimate more accurately nano-crystallite size using XRD. *World J. Nano Sci. Eng.* **2012**, *2*, 154-160, https://doi.org/10.4236/wjnse.2012.23020.

26. El haimer, C, ; Lghazi, Y; Bahar, J; Youbi, B; Ait himi, M; Ouedrhiri, A Aynaou, A; Bimaghra, I «Investigation of nucleation and growth mechanism of selenium electrodeposited on ITO substrate», *Mater. Today*, **2022**, *66*, 37-44. https://doi.org/10.1016/j.matpr.2022.03.107.
27. Zebbar, N.; Aida, M.S.; Hafdallah, A.E.K.; Daranfad, O.; Lekiket, H.; Kechouane, M. Properties of ZnO thin films grown on Si substrates by ultrasonic spray and ZnO/Si heterojunctions. *Mater. Sci. Forum.* **2009**, *609*, 133-137, https://doi.org/10.4028/www.scientific.net/MSF.609.133.